Petrophysical Properties and Permeability Prediction for the Abu Madi Formation, Baltim North Gas Field, Nile Delta, Egypt

Abdel Moktader A. El Sayed[1], Samy Zayed[2], Amir M. S. Lala[1], Nahla A. El Sayed[3], Ahmed Salah[2]

(1) Department of Geophysics, Ain Shams University, Cairo, Egypt
(2) Belayim Petroleum Company, Nasr City, Cairo, Egypt
(3) Egyptian Petroleum Research Institute, Department of Core analysis, Nasr City, Egypt
Corresponding Author: Abdel Moktader A. El Sayed1

ABSTRACT

Drilling, coring, and geophysical logging were performed with a seafloor drilling rig to investigate a potentially gas occurrences of the Nile deep sea fan, in Baltim North Gas Field, Nile Delta, Egypt. Different sites within stream-mouth bar genetic deltaic units were investigated. Geophysical log data of electrical resistivity, Neutron, Density, NMR and spectral gamma ray are combined with core-derived physical properties of porosity, permeability, electrical resistivity, MICP and bulk density. Core- and log physical property data are used to define NMR-T2 conversion by empirical modeling, which is then used to interpret the permeability data in non-cored wells.

The mercury injection capillary pressure (MICP) measurements for some selected samples have been used to evaluate both reservoir micro and macro porosity cut off values. Three reservoir flow units which have been detected based on the integration of pore throat radius (r35) and NMR T2-cutoff are related to only two superimposed stream-mouth bar genetic deltaic units having been penetrated in Baltim North-5st well. It is of highly beneficial for permeability prediction in other un-cored drilled wells in the Baltim gas field. The intercorrelation among core-derived physical properties and borehole log data gives an opportunity to determining the permeability profile side by side with Swi for each detected rock flow unit in un-cored well. It has been done through the calculated regression line models, connected to different flow units, in the studied cored wells.

Verification of permeability prediction obtained models has been approved through the correlation between the predicted permeability and the permeability derived from normalized NMR -T2 cutoff (150μm). It shows a robust and reliable coefficient of correlation (R= 0.91). The predicted and calculated permeabilities showed a close matching with each other. The lake of the associated water production confirms that most of the calculated water saturation was mainly irreducible.

Date of Submission: 20-06-2020   Date of Acceptance: 07-07-2020

I. INTRODUCTION

The permeability prediction remains a great challenge for most reservoir rocks. Several studies have been introduced by many authors; El Sayed,(1993), Glover, et al.,(2006), Halisch et al.(2009); Aagaard (2010), Rikke, et al (2017), Zhu, et al.,(2017), Lala and El-Sayed (2017), Xuqiang Fan, et al.,(2019), and Al Khalifa, et al.,(2020). Most of them tried successfully to link core Laboratory measurements to the conventional downhole petrophysical properties. To achieve the goal of the present work, porosity-permeability core data, Neutron-Density logs, applying the reservoir flow units concepts, analysis of the results of well log Nuclear Magnetic Resonance (NMR), modeling the well logs resistivity to quantitatively estimate the permeability of the reservoir based on the petrophysical properties of the rocks to overcome the lack of coring due to its highly cost in the Nile Delta offshore.

The Nile Delta area is the oldest gas provinces in Egypt, as its sedimentary successions contain a high gas potentiality. Offshore Egypt in the south-eastern Mediterranean area hosts the prolific West Delta Deep Marine concession with extensive commercial production. Non-associated gas is produced in the northern Western Desert of Egypt and in the offshore extension of the Nile Delta in the East-Mediterranean. The offshore East-Mediterranean region accounts for about 60% of Egypt's 223 billion cubic feet (bcf) of proven natural gas reserves and nearly six million barrels of natural gas liquids (El Diasty, 2010 and El Diasty, et al, 2020).

The Baltim Fields (Figure 1) were discovered by IEOC in 1993 through Baltim East-1 well and in 1995 through Baltim North-1 well. Up to date 12 wells have been drilled in the Baltim East and 7 in the Baltim North.

They are producing from the Abu Madi Formation of the Late Messinian age. The stratigraphic units of the Neogene-Quaternary succession of the study area are shown in Figure-2.
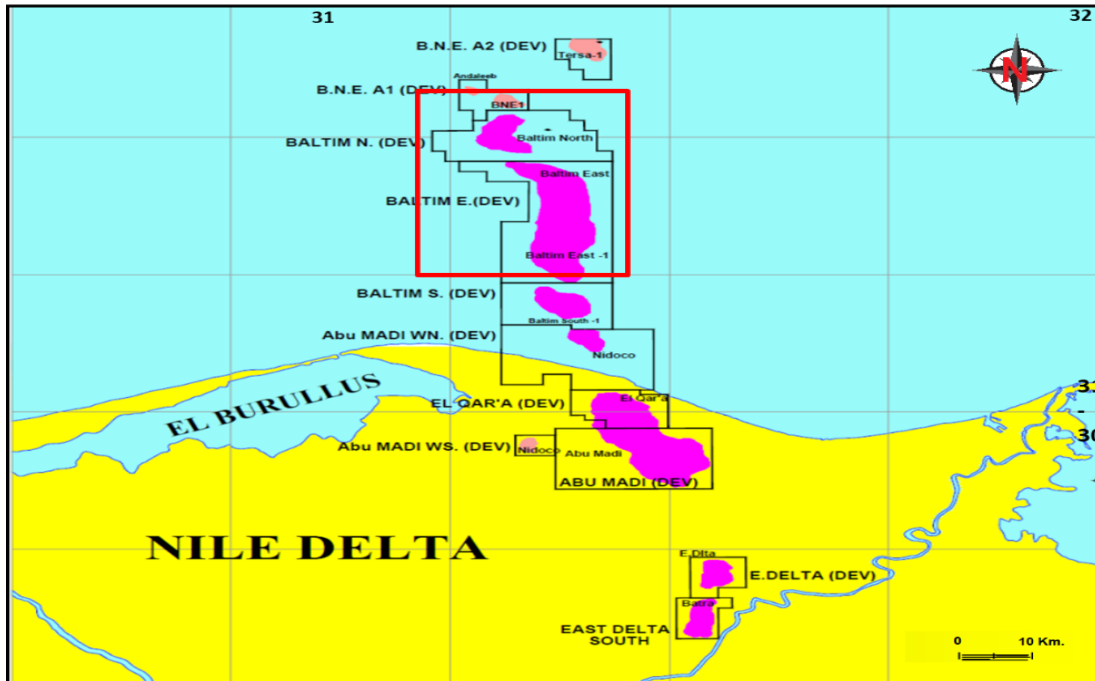
Fig. 1: Location map for the study area.

The importance of the Abu Madipaleo-valley dated back to sixties (1967) when the Nile Delta basin discovered as of high hydrocarbon gas potentiality in Abu Madi gas field in the onshore area and Abu Qir gas field in the offshore area. In both fields, gas was produced from the Abu Madi Formation. It is subdivided into three levels, while the level III main was the target in the Baltim North Field. This level is mainly sandstone deposited in delta environment and consists of different superimposed reservoir flow zones. The change in depositional setting for each sandstone type establishes certain variation in porosity and permeability within the same facies type. The permeability may indicate low values due to the presence of bioturbation and increased mud content owing to the burrows with bimodal grain classification, regardless of change in gamma ray readings. This phenomenon signifies that there exists no strict correlation between gamma ray and permeability profile (Numair et.al., 2020) despite containing good quality reservoir rocks.
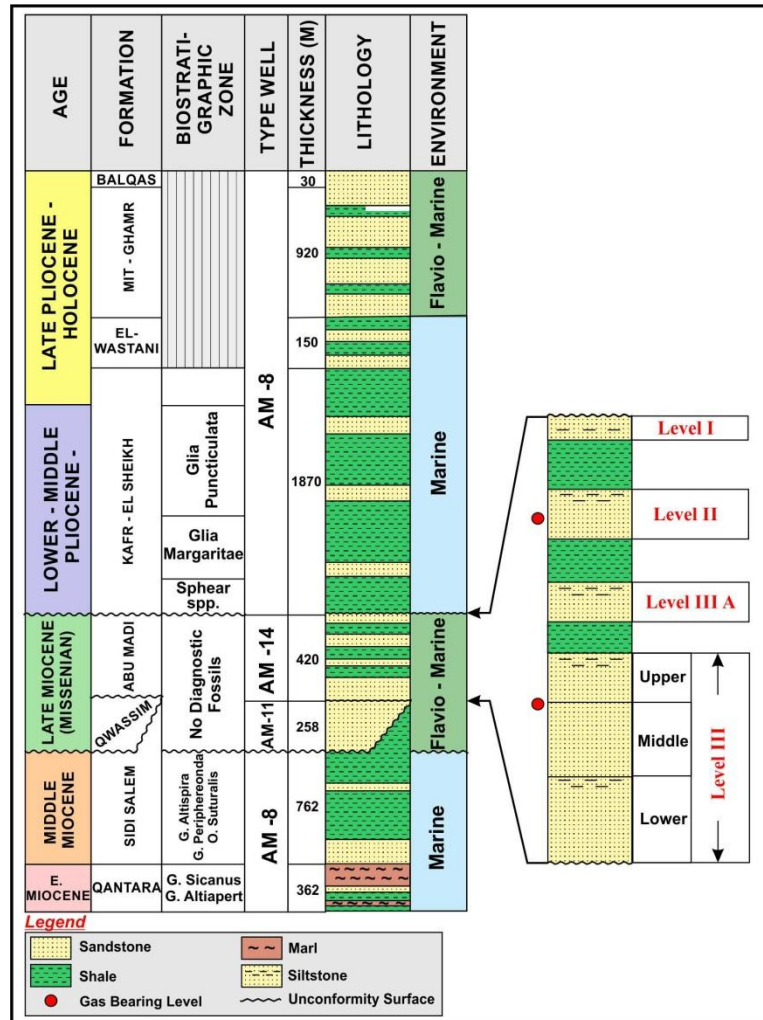
Fig. 2: Stratigraphic Column of Baltim Fields, Nile Delta (El Heiny et al., 1990).

The main target of the present study was a trial for anatomy of the Abu Madi reservoir rocks encountered in the Baltim North gas field by detecting its flow units, based on the integration of core analysis data (r35) with the NMR-T2 log results to obtain reliable relations helping for permeability prediction in each detected flow unit to calculate permeability in the un-cored boreholes. In addition, to build petrophysical models for permeability prediction in non-cored wells. Verification of core-permeability prediction models with log estimated permeability is consequent target as well.

II.   MATERIAL AND METHODS

This study has been carried out using Baltim North-5st well (where core data are available) and Baltim North-6 (un-cored well). The available log suite in well Baltim North-5st is Gamma Ray, Resistivity, Density and Neutron. In addition, a core has been cut in level III main (35.5 m with 100% recovery). The available logs in the second well Baltim North-6 are GR, Resistivity and NMR.

1. Core sample preparation:
1.1 Core cutting
113 core plugs were drilled from the full diameter cores obtained from Abu Madi Formation. Plugs of 2.5 cm diameter and 3.5-4.5cm in length were cut for both parallel samples (parallel to the bedding plane) every 25 cm and/or perpendicular to the bedding plane, everyone meter through the full-diameter core intervals.
The core plug samples were trimmed to produce right cylinders, and the trims labelled and boxed for subsequent use. The rest of drilled cylinders were used for petrographical and mineralogical examinations (Thin sections and XRD).

1.2 Core cleaning and drying

The plug samples were cleaned in hot refluxing solvents (Toluene and Methanol) by using Soxhlet Extractor Apparatus and dried in a regular oven at 87-90°C. Toluene is used to remove all hydrocarbons from the plug. The plug was considered as residual hydrocarbon free after examination by the Ultraviolet light lamp.

Methanol was used to remove the salt from the plugs, and the cleaning process was complete when silver nitrate (as indicator) did not react with the solvent (Methanol), which means that the solvent no longer has any salts.

1.3 Core analysis measurements.

Weight, length, and diameter of each plug were measured using electric balance and Verner. 113 Core samples obtained from Abu Made Formation were subjected for porosity and permeability measurements using Helium porosimeter and Ruska gas permeameter, respectively. Porosity and permeability values were determined at ambient conditions. Also, grain density and bulk density were determined during the same process.

Some core samples of different porosity, density and permeability were selected to perform special core analyses. The special core analyses were including formation resistivity factor (FF) and formation resistivity index (RI) at room and overburden reservoir pressure at formation water concentration. The Mercury injection capillary pressure (MICP) and pore size distribution up to 60,000psi were measured.

III. RESULTS AND DISCUSSIONS

a. Petrographical investigation:

The distribution of the remaining hydrocarbon in developed oilfields is primarily influenced by the existing diagenetic reservoir facies, which include the effects of both the sedimentary environment and the local diagenetic processes on the reservoir quality. The mineralogical, petrographic descriptions and X-Ray diffraction (XRD) analysis for some selected samples obtained from well Baltim North-5st well show that the majority of studied samples are mainly composed from quartz and few feldspars as detrital grains and cemented by calcite. In addition, Fe-calcite and few dolomite contents associated with some clays (chlorite) were observed which could be classified as of authigenic origin (Figure 3). Both detrital and authigenic minerals were outlined as shown in Table (1). Chlorite grain coatings in sandstones (Fig.3D) can inhibit quartz overgrowths and preserve porosity in theAbu Madi reservoirs, butcoatings may also introduce high irreducible water saturation (Swi) and therefore reduce effective porosity (Haoran et al.,2020).

Wei Meng et al.,(2020) stated that the main diagenetic product of feldspar transformation, is namely authigenic kaolinite. The presence of authigenic kaolinite in terms of the physical and chemical features acts as indicators of the transformation process of feldspar and the consequent formation of secondary pores (Fig.3 B,C&D). In the present work, the K-feldspar (Fig.3C) is transformed into kaolinite accompanied by dissolution of carbonate cements (Calcite, Fig. A& C) and accompanied by consequent formation and preservation of secondary pores.
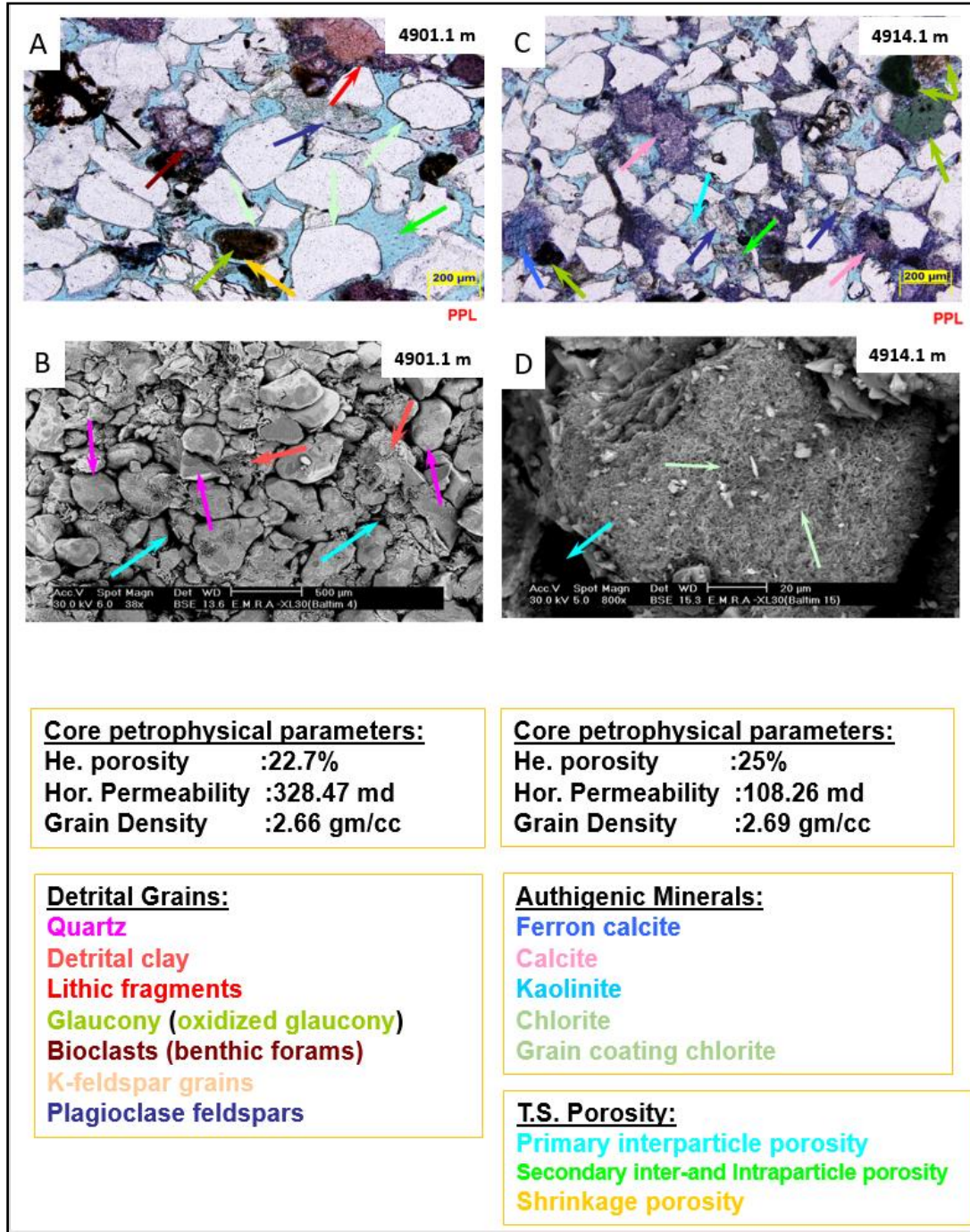
Fig. 3: Photomicrograph and SEM showing the main detrital grains, authigenic minerals and porosity in the studied Level III Main, Baltim- North-5st well (Color of authigenic minerals, detrital grains and porosity type belongs to the arrow color).

Tab. 1: XRD and Petrographic analyses for samples of Baltim North-5st

Detrital Grains		Authigenic Minerals	
Quartz	77 %	Calcite	16%
Feldspar	3%	Dolomite	2%
		Chlorite	2%

s. no.1(4901m-red) and s. no.2 (4914m-blue)
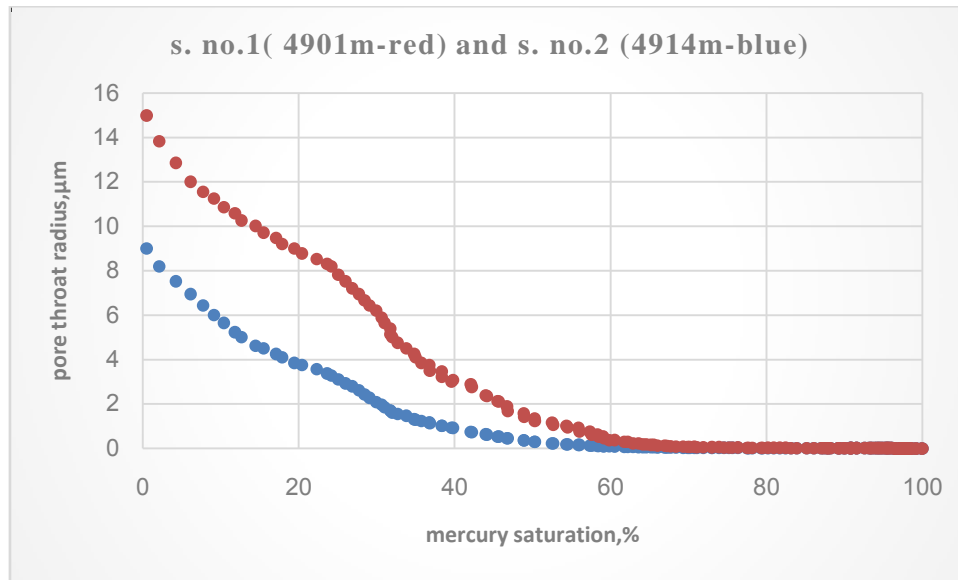
b. Rock density determination:

Although the standard sandstone grain density is usually used to calculate porosity from density log is 2.65 gm/cc, the laboratory measurements of the Abu Madi sandstones show higher values. The measured grain density (> 2.73 gm/cc) in some core samples as shown in Table 2 and Table 3 and Figure 5.It may be due to the presence of detrital oxidized glauconitic as predominant detrital mineral (Figs.3A&C).

Tab. 2: Grain density and bulk density measurements for Core-1 in well Baltim North-5st

Sample No.	Depth, (m)	Grain Density, (gm/cc)	Dry Bulk Density, (gm/cc)	Sample No.	Depth, (m)	Grain Density, (gm/cc)	Dry Bulk Density, (gm/cc)
1	4898.02	2.71	2.19	37	4907.02	2.70	2.00
2	4898.32	2.67	2.11	38	4907.27	2.70	2.56
3	4898.52	2.68	1.96	39	4907.52	2.69	2.19
4	4898.79	2.68	1.98	40	4907.77	2.68	2.05
5	4899.03	2.68	2.42	41	4908.02	2.68	2.04
6	4899.28	2.67	1.96	42	4908.32	2.69	2.09
7	4899.70	2.70	1.97	43	4908.52	2.69	2.13
8	4899.82	2.67	2.07	44	4908.80	2.69	2.12
9	4900.03	2.69	2.06	45	4909.03	2.67	1.92
10	4900.27	2.70	2.01	46	4909.44	2.69	2.10
11	4900.53	2.70	2.02	47	4909.61	2.69	2.07
12	4900.83	2.66	1.96	48	4909.77	2.70	1.96
13	4901.03	2.69	2.48	49	4910.02	2.72	2.23
14	4901.30	2.66	1.99	50	4910.28	2.71	2.02
15	4901.53	2.66	2.06	51	4910.58	2.71	2.03
16	4901.81	2.68	2.09	52	4910.77	2.72	2.06
17	4902.12	2.68	2.09	53	4911.12	2.71	2.43
18	4902.27	2.66	2.00	54	4911.33	2.74	2.35
19	4902.52	2.68	2.03	55	4911.64	2.73	2.34
20	4902.77	2.68	2.02	56	4911.82	2.72	2.38
21	4903.02	2.67	2.08	57	4912.06	2.68	2.10
22	4903.30	2.67	2.00	58	4912.27	2.69	2.02
23	4903.63	2.65	2.00	59	4912.62	2.70	2.09
24	4903.82	2.68	2.01	60	4912.77	2.69	2.03
25	4904.05	2.68	1.98	61	4913.02	2.69	2.07
26	4904.35	2.69	2.43	62	4913.27	2.72	2.18
27	4904.52	2.68	2.02	63	4913.52	2.71	2.10
28	4904.81	2.70	2.25	64	4913.79	2.69	2.01
29	4905.03	2.68	2.09	65	4914.02	2.68	1.98
30	4905.27	2.68	2.00	66	4914.33	2.69	2.06
31	4905.52	2.67	2.11	67	4914.52	2.69	1.94
32	4905.90	2.67	2.05	68	4914.80	2.69	1.98
33	4906.02	2.68	2.00	69	4915.02	2.69	1.99
34	4906.43	2.70	2.01	70	4915.32	2.68	2.02
35	4906.65	2.69	1.98	71	4915.55	2.69	2.06
36	4906.77	2.70	2.02	72	4915.81	2.70	2.11

The bulk density – porosity relation (Fig. 4) shows a very close correlation permits calculation of porosity from bulk density. This relation is controlled by a very reliable regression line equation (R^2 = 0.991).

$\rho B = -0.0282\emptyset +2.7199$…………… (1)

The grain - bulk density relation (Figure 5) shows an increasing of bulk density by the increase of grain density. The calculated regression line equation is characterized by a fair coefficient of correlation (R=0.51).

c.   Correction of Porosity according to reservoir overburden:

The core porosity (ambient) has been laboratory measured for all samples at room conditions, while only 28 selected samples (representing different porosity values) were measured at reservoir overburden pressure (6000 Psi ,table 4) to study the effect of compaction on the rock porosity.

Tab. 3: Grain density and bulk density measurements for Core-2 in well Baltim North 5st

Sample No.	Depth, (m)	Grain Density, (gm/cc)	Dry Bulk Density, (gm/cc)	Sample No.	Depth, (m)	Grain Density, (gm/cc)	Dry Bulk Density, (gm/cc)
73	4916.03	2.69	1.99	94	4921.32	2.70	2.46
74	4916.43	2.69	2.01	95	4921.55	2.67	1.90
75	4916.52	2.68	1.94	96	4921.80	2.69	2.01
76	4916.92	2.69	2.03	97	4922.05	2.68	1.99
77	4917.03	2.70	2.07	98	4922.31	2.69	1.99
78	4917.26	2.70	2.00	99	4922.57	2.70	2.00
79	4917.54	2.70	2.03	100	4922.80	2.69	2.06
80	4917.92	2.69	1.99	101	4923.18	2.73	2.26
81	4918.17	2.67	1.94	102	4923.40	2.68	2.06
82	4918.28	2.69	1.92	103	4923.57	2.66	1.94
83	4918.52	2.69	2.01	104	4923.86	2.70	2.02
84	4918.86	2.68	2.05	105	4924.10	2.70	2.04
85	4919.18	2.66	1.94	106	4924.36	2.70	2.08
86	4919.34	2.69	1.99	107	4924.70	2.74	2.28
87	4919.72	2.69	2.08	108	4924.81	2.71	2.16
88	4919.92	2.69	1.99	109	4925.18	2.71	2.08
89	4920.07	2.70	2.02	110	4925.31	2.72	2.12
90	4920.42	2.70	1.99	111	4925.54	2.71	2.05
91	4920.52	2.68	1.98	112	4925.83	2.72	2.12
92	4920.87	2.70	2.03	113	4926.10	2.73	2.34
93	4921.02	2.68	2.03				

Fig. 4: Grain density determination from core data in Baltim North-5st well.

The porosity at reservoir overburden was less by about 5% compared to the ambient porosity. The porosity discrepancy could be explained by its negative impact on the log-estimated water saturation profile, as it appears higher than it should be.
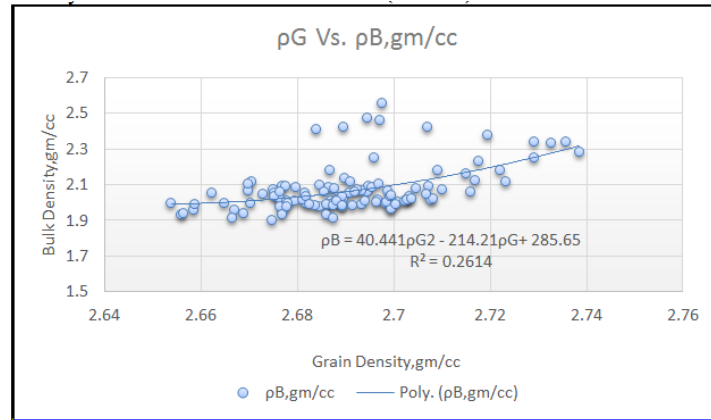
Fig. 5: Bulk versus Grain Density of Abu Madi Reservoir Rocks.

Tab. 4: Core porosity measurements of some selected samples at ambient and overburden pressure for the Baltim North-5st well (Core 1 and 2).

Sampl No.	Depth (meter)	Helium Porosity (%)		Sampl No.	Depth (meter)	Helium Porosity (%)	
		Ambient	Overburden 6000			Ambient	Overburden 6000
1E	4901.49	24.50	22.70	1P	4898.35	20.5	19.3
2E	4904.10	25.10	23.40	2P	4900.38	22.00	20.70
3E	4905.16	22.30	20.80	3P	4902.13	19.90	19.10
4E	4909.19	24.70	23.30	4P	4905.11	22.50	20.60
5E	4916.14	25.20	23.40	5P	4906.53	19.60	17.40
6E	4922.20	24.90	23.40	6P	4908.15	20.10	19.00
1F	4898.55	25.40	23.40	7P	4910.17	19.10	17.60
2F	4900.35	23.70	21.70	8P	4913.12	21.10	19.90
3F	4904.05	12.90	11.30	9P	4918.10	25.30	23.50
4F	4906.30	25.40	23.50	10P	4924.08	21.00	19.80
5F	4908.12	21.30	19.60	1R	4899.25	25.30	23.50
6F	4914.20	25.60	23.70	2R	4903.40	23.70	22.50
7F	4919.08	27.30	25.20	3R	4908.97	26.90	25.30
8F	4923.17	16.00	15.10	4R	4923.58	27.20	24.90

The relationship between the Abu Madi Formation porosity at ambient and at reservoir overburden conditions is shown in (Figure 6), while the calculated regression line equation representing this relation is:
$$\text{Ø}_r = 0.9401\,\text{Ø}_a - 0.2385\ldots\ldots \qquad\qquad \ldots\ldots\ldots (2)$$

Where: **Ø$_r$** is the porosity measured under overburden pressure and **Ø$_a$** is the porosity measured at room conditions. The calculated regression equation (2) is characterized by a very high coefficient of correlation ($R^2 = 0.9895$) permits to calculate one porosity from the other with high precession.

This equation (2) has been used to correct all the core porosity data from ambient to the net reservoir overburden porosity. The correction was essential to correlate the log porosity with core porosity in the Baltim field.
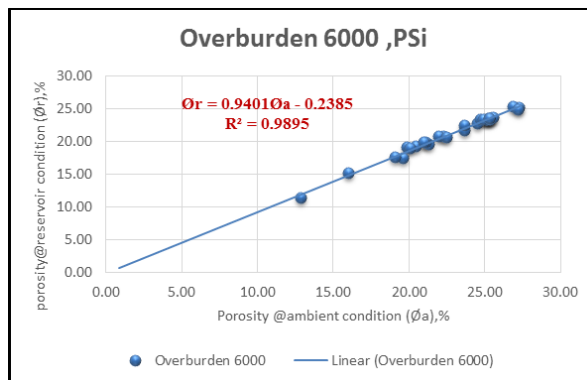
Fig. 6: Corrected core porosity for uniaxial stress versus porosity at ambient condition for Abu Madi Formation - Baltim North-5st well.

d.   Electrical Properties:

The electrical measurements were conducted for the Abu Madi core samples obtained from the Baltim North-5st well. The calculated cementation factor (m) ranges from 1.45 up to 1.61 (Figure 9) at ambient and reservoir pressure (6600 Psi), while formation water (Rw) = 0.3523ohm.m.It is noticed that (m) increases with pressure increase. The Archie's multiplier (a) increases from 1.62 (ambient) up to 1.68 (reservoir conditions, see Figure 7). The calculated Archie's second equation under Abu Madi reservoir pressure is;

$$F = 1.67 \, \varnothing^{-1.61} \ldots\ldots\ldots \qquad\qquad\qquad \ldots (3)$$

Where m = 1.61 and a = 1.67

The saturation exponent (n) is estimated through the measurement of the electrical resistivity of both fully and partial saturated core samples (Ro&Rt) with water saturation determination in each step using the centrifuge method.The polygonal distribution of the saturation exponent (n) exposes its normal unimodal distribution with mean value equals 1.963.(Fig. 8)

The values of both (m and n) have been used as an Archie's 2nd equations ($F = a \, \varnothing^{-m}$ and $RI = c \, Sw^{-n}$) as references inputs during Abu Madi reservoir evaluation and fluid saturation calculations using software. The calculated resistivity index-water saturation relation for the Abu Madi reservoir is;

$$RI = 1.0 \, Sw^{-1.96} \ldots\ldots\ldots \qquad\qquad\qquad \ldots (4)$$

Where n = 1.96 and c = 1.0
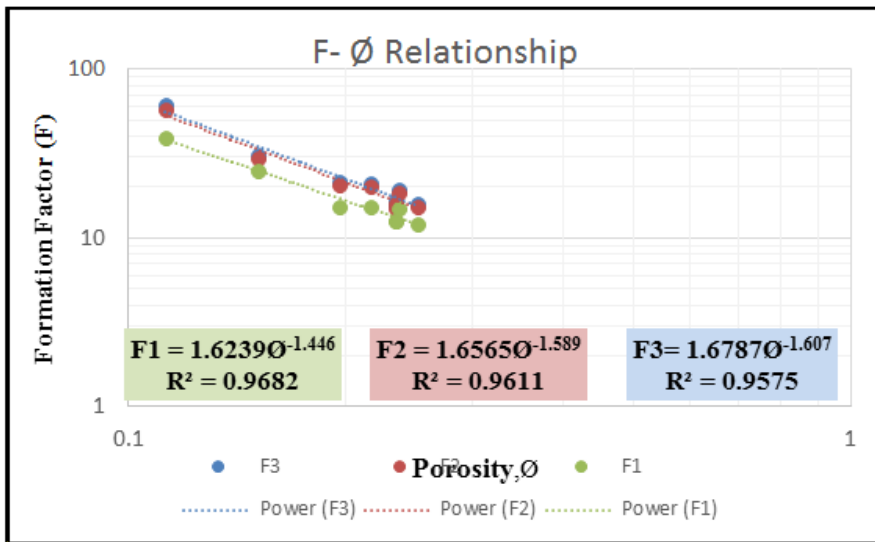
Fig. 7: Cementation factor (m) determination in the Baltim North-5st well.
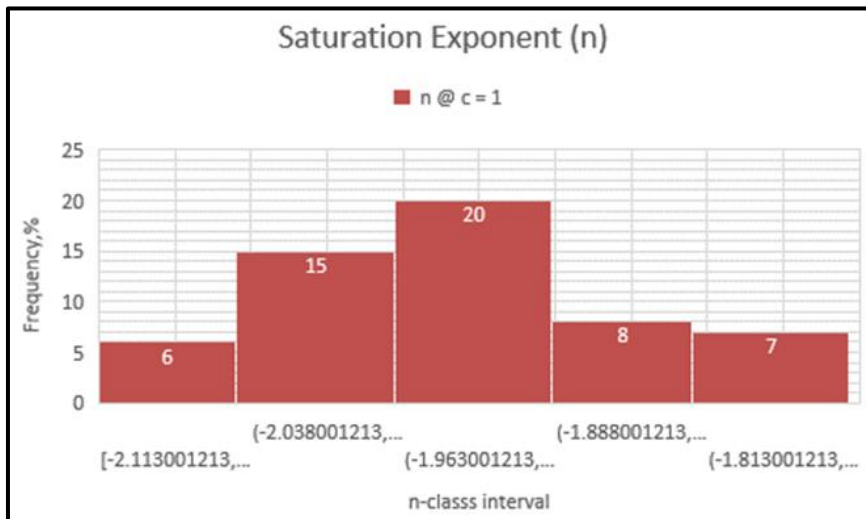
Fig. 8: Estimated Saturation Exponent (n) Polygon in the Baltim North-5st well.

e.   Micro porosity from mercury injection capillary pressure (MICP):

Mercury injection capillary pressure (MICP) data for core samples of the Baltim North-5st well were used to estimate the pore throat size distribution (PTSD) and to discriminate the micro and macro porosity. Tables 5 and 6 represent the MICP for the two selected core samples. (Samples no. 1E and 5E). It is assumed that micro porosity is the volume represents irreducible water saturation and macro porosity is the volume represents the amount of movable fluids (**El Sayed, et al, 2005**).

The MICP results expose that irreducible water saturation (SWi) is reaching values up to 45% in some samples (S. No. 5E) as a value of the high micro-porosity component respect to the pore throat radius distribution observed in the core No.1.(Figure 9). The pore throat cutoff value is ranged from 0.2 up to 0.9μm in the studied samples (Samples no. 1E and 5E).

Tab. 5: Mercury Injection capillary pressure measurements for sample no. 1E in Baltim North-5st well.

Mercury Injection Pressure (psia)	Pore Throat Radius (μm)	Mercury Saturation (Fraction)	Pore Throat Radius Distrib'n	Equivalent Water Saturation (Fraction)	Mercury Injection Pressure (psia)	Pore Throat Radius (μm)	Mercury Saturation (Fraction)	Pore Throat Radius Distrib'n	Equivalent Water Saturation (Fraction)	Mercury Injection Pressure (psia)	Pore Throat Radius (μm)	Mercury Saturation (Fraction)	Pore Throat Radius Distrib'n	Equivalent Water Saturation (Fraction)
94.91	0.953	0.613	0.130	0.387	7986.79	0.011	0.944	0.080	0.056	5.54	16.334	0.000	0.000	1.000
96.83	0.934	0.614	0.115	0.386	8486.53	0.011	0.948	0.072	0.052	6.04	14.984	0.004	0.091	0.996
119.95	0.754	0.630	0.108	0.370	8985.51	0.010	0.950	0.082	0.050	6.53	13.838	0.011	0.196	0.989
122.09	0.741	0.632	0.108	0.368	9486.97	0.010	0.954	0.090	0.046	7.04	12.852	0.022	0.354	0.978
146.54	0.617	0.645	0.106	0.355	9985.30	0.009	0.957	0.077	0.043	7.54	12.001	0.045	0.541	0.955
147.49	0.613	0.645	0.101	0.355	10486.89	0.009	0.960	0.061	0.040	7.82	11.565	0.063	0.689	0.937
168.95	0.535	0.655	0.090	0.345	10984.45	0.008	0.961	0.058	0.039	8.03	11.257	0.077	0.787	0.923
172.08	0.526	0.655	0.079	0.345	11485.41	0.008	0.964	0.056	0.036	8.32	10.873	0.096	0.885	0.904
197.39	0.458	0.663	0.080	0.337	11987.11	0.008	0.964	0.060	0.036	8.53	10.596	0.113	0.984	0.887
243.59	0.371	0.676	0.081	0.324	12484.14	0.007	0.967	0.062	0.033	8.82	10.258	0.138	1.000	0.862
247.29	0.366	0.676	0.076	0.324	12982.68	0.007	0.968	0.041	0.032	9.03	10.012	0.154	0.953	0.846
295.35	0.306	0.685	0.076	0.315	13483.55	0.007	0.969	0.029	0.031	9.31	9.709	0.173	0.923	0.827
298.41	0.303	0.686	0.082	0.314	13982.19	0.006	0.969	0.044	0.031	9.53	9.486	0.189	0.924	0.811
392.91	0.230	0.702	0.085	0.298	14481.91	0.006	0.971	0.041	0.029	9.81	9.216	0.205	0.963	0.795
396.28	0.228	0.703	0.084	0.297	14981.05	0.006	0.971	0.034	0.029	10.03	9.015	0.223	0.982	0.777
492.89	0.183	0.715	0.085	0.285	15483.02	0.006	0.971	0.061	0.029	10.31	8.771	0.241	0.928	0.759
497.15	0.182	0.716	0.089	0.284	15979.41	0.006	0.975	0.066	0.025	10.59	8.539	0.257	0.861	0.743
592.27	0.153	0.727	0.091	0.273	16478.98	0.005	0.975	0.041	0.025	10.87	8.318	0.272	0.784	0.728
596.05	0.152	0.727	0.091	0.273	16979.67	0.005	0.976	0.036	0.024	11.03	8.199	0.280	0.687	0.720
691.40	0.131	0.736	0.091	0.264	17480.75	0.005	0.977	0.033	0.023	11.56	7.824	0.300	0.629	0.700
696.17	0.130	0.737	0.091	0.263	17980.18	0.005	0.977	0.022	0.023	12.03	7.518	0.318	0.599	0.682
798.23	0.113	0.745	0.093	0.255	18478.84	0.005	0.978	0.014	0.022	12.56	7.202	0.335	0.559	0.665
898.19	0.101	0.753	0.094	0.247	18980.11	0.005	0.978	0.017	0.022	13.03	6.942	0.349	0.516	0.651
999.43	0.090	0.760	0.096	0.240	19479.20	0.005	0.978	0.035	0.022	13.55	6.673	0.362	0.478	0.638
1099.54	0.082	0.767	0.098	0.233	19979.10	0.005	0.979	0.038	0.021	14.02	6.448	0.373	0.444	0.627
1197.34	0.076	0.773	0.100	0.227	20986.97	0.004	0.980	0.031	0.020	14.55	6.216	0.384	0.409	0.616
1299.33	0.070	0.778	0.100	0.222	21990.06	0.004	0.981	0.042	0.019	15.33	5.901	0.398	0.380	0.602
1400.61	0.065	0.784	0.097	0.216	22992.21	0.004	0.983	0.048	0.017	16.02	5.644	0.409	0.357	0.591
1498.09	0.060	0.788	0.103	0.212	23992.83	0.004	0.984	0.033	0.016	16.80	5.384	0.421	0.337	0.579
1593.00	0.057	0.792	0.113	0.208	24994.31	0.004	0.985	0.016	0.015	17.57	5.146	0.431	0.314	0.569
1695.03	0.053	0.798	0.107	0.202	25993.66	0.003	0.985	0.015	0.015	18.02	5.017	0.436	0.289	0.564
1796.68	0.050	0.801	0.103	0.199	26994.11	0.003	0.985	0.028	0.015	19.05	4.748	0.447	0.269	0.553
1896.93	0.048	0.806	0.110	0.194	27995.39	0.003	0.987	0.035	0.013	20.02	4.516	0.456	0.256	0.544
1999.62	0.045	0.810	0.112	0.190	28995.70	0.003	0.987	0.032	0.013	21.29	4.247	0.467	0.243	0.533
2197.89	0.041	0.817	0.110	0.183	29996.89	0.003	0.988	0.031	0.012	22.02	4.107	0.472	0.231	0.528
2397.09	0.038	0.824	0.112	0.176	30996.25	0.003	0.988	0.032	0.012	23.54	3.842	0.483	0.219	0.517
2592.60	0.035	0.830	0.120	0.170	31995.88	0.003	0.990	0.035	0.010	24.02	3.765	0.486	0.207	0.514
2795.17	0.032	0.836	0.127	0.164	32996.37	0.003	0.990	0.038	0.010	25.79	3.507	0.495	0.198	0.505
2989.91	0.030	0.843	0.135	0.157	33995.98	0.003	0.991	0.037	0.009	26.02	3.476	0.497	0.189	0.503
3239.14	0.028	0.850	0.141	0.150	34996.63	0.003	0.991	0.038	0.009	28.02	3.228	0.506	0.226	0.494
3491.19	0.026	0.859	0.142	0.141	35996.61	0.003	0.992	0.039	0.008	30.01	3.013	0.515	0.274	0.485
3740.23	0.024	0.863	0.152	0.137	36996.78	0.002	0.993	0.035	0.007	30.73	3.085	0.517	0.213	0.483
3985.54	0.023	0.873	0.159	0.127	37996.98	0.002	0.993	0.060	0.007	31.88	2.896	0.521	0.118	0.479
4475.17	0.020	0.884	0.155	0.116	38996.80	0.002	0.995	0.094	0.005	32.76	2.760	0.524	0.095	0.476
4490.50	0.020	0.885	0.160	0.115	39996.74	0.002	0.998	0.071	0.002	37.82	2.391	0.534	0.106	0.466
4735.02	0.019	0.890	0.169	0.110	41996.37	0.002	0.998	0.032	0.002	38.33	2.359	0.535	0.118	0.465
4986.57	0.018	0.898	0.170	0.102	43996.59	0.002	0.999	0.019	0.001	42.32	2.137	0.543	0.118	0.457
5234.71	0.017	0.902	0.174	0.098	45996.38	0.002	1.000	0.009	0.000	42.75	2.116	0.544	0.108	0.456
5483.75	0.016	0.909	0.185	0.091	47995.55	0.002	1.000	0.001	0.000	48.09	1.881	0.553	0.108	0.447
5732.35	0.016	0.914	0.183	0.086	49994.94	0.002	1.000	0.000	0.000	53.62	1.686	0.560	0.124	0.440
5986.04	0.015	0.920	0.168	0.080	51993.95	0.002	1.000	0.000	0.000	57.19	1.581	0.567	0.136	0.433
6237.54	0.014	0.924	0.150	0.076	53989.17	0.002	1.000	0.000	0.000	63.22	1.430	0.577	0.129	0.423
6485.51	0.014	0.928	0.135	0.072	55986.46	0.002	1.000	0.001	0.000	66.56	1.359	0.581	0.123	0.419
6734.27	0.013	0.931	0.126	0.069	57985.09	0.002	1.000	0.003	0.000	73.24	1.235	0.589	0.131	0.411
6984.20	0.013	0.934	0.131	0.066	59985.22	0.002	1.000	0.001	0.000	77.20	1.171	0.594	0.132	0.406
7212.77	0.013	0.937	0.130	0.063						84.83	1.066	0.604	0.122	0.396
7486.32	0.012	0.942	0.105	0.058						88.51	1.022	0.605	0.127	0.395

Tab. 6: Mercury Injection capillary pressure measurements for sample no. 5E in Baltim North-5st well.

Mercury Injection Pressure (psia)	Pore Throat Radius (µm)	Mercury Saturation (Fraction)	Pore Throat Radius Distrib'n	Equivalent Water Saturation (Fraction)
9.54	9.484	0.000	0.000	1.000
10.03	9.013	0.005	0.352	0.995
11.03	8.198	0.021	0.572	0.979
12.03	7.517	0.042	0.660	0.958
13.03	6.942	0.061	0.651	0.939
14.03	6.447	0.077	0.607	0.923
15.05	6.008	0.091	0.580	0.909
16.02	5.643	0.104	0.565	0.896
17.30	5.228	0.118	0.569	0.882
18.03	5.016	0.126	0.637	0.874
19.55	4.625	0.144	0.761	0.856
20.02	4.516	0.154	0.707	0.846
21.29	4.247	0.170	0.749	0.830
22.02	4.106	0.178	0.730	0.822
23.54	3.842	0.194	0.881	0.806
24.02	3.765	0.204	1.000	0.796
25.29	3.576	0.223	0.872	0.777
26.85	3.368	0.236	0.664	0.764
27.54	3.284	0.242	0.534	0.758
29.04	3.114	0.251	0.466	0.749
30.96	2.921	0.260	0.456	0.740
32.42	2.789	0.268	0.433	0.732
34.43	2.627	0.277	0.354	0.723
37.17	2.433	0.284	0.289	0.716
39.82	2.271	0.290	0.287	0.710
43.24	2.091	0.299	0.297	0.701
45.79	1.975	0.306	0.268	0.694
48.58	1.862	0.310	0.237	0.690
52.70	1.716	0.317	0.208	0.683
53.09	1.703	0.317	0.201	0.683
55.98	1.615	0.320	0.314	0.680
58.04	1.558	0.326	0.422	0.674
61.85	1.462	0.338	0.376	0.662
69.33	1.304	0.348	0.356	0.652
69.75	1.297	0.350	0.437	0.650
72.90	1.241	0.357	0.448	0.643
78.01	1.159	0.367	0.397	0.633
79.54	1.137	0.368	0.382	0.632
88.06	1.027	0.383	0.390	0.617
88.59	1.021	0.383	0.391	0.617
96.48	0.937	0.395	0.370	0.605
98.60	0.917	0.397	0.335	0.603
121.37	0.745	0.421	0.316	0.579
123.01	0.735	0.422	0.310	0.578
144.09	0.628	0.439	0.298	0.561
147.89	0.611	0.441	0.286	0.559
169.54	0.533	0.455	0.272	0.545
172.68	0.524	0.456	0.254	0.544
195.19	0.463	0.467	0.255	0.533
197.92	0.457	0.468	0.268	0.532
242.47	0.373	0.488	0.252	0.512
248.18	0.364	0.489	0.223	0.511
296.33	0.305	0.502	0.223	0.498
297.41	0.304	0.503	0.233	0.497
391.27	0.231	0.525	0.233	0.475
396.79	0.228	0.526	0.233	0.474
492.10	0.184	0.544	0.235	0.456
497.19	0.182	0.545	0.236	0.455
591.92	0.153	0.559	0.247	0.441
596.71	0.152	0.560	0.275	0.440
690.40	0.131	0.573	0.273	0.427
696.29	0.130	0.576	0.224	0.424
790.52	0.114	0.583	0.180	0.417
798.36	0.113	0.584	0.169	0.416
895.15	0.101	0.590	0.180	0.410
897.38	0.101	0.591	0.193	0.409
998.72	0.091	0.598	0.223	0.402
1099.21	0.082	0.605	0.275	0.395
1196.14	0.076	0.617	0.275	0.383
1300.19	0.070	0.622	0.251	0.378
1399.04	0.065	0.629	0.263	0.371
1497.27	0.060	0.636	0.259	0.364
1598.96	0.057	0.641	0.243	0.359
1695.26	0.053	0.646	0.245	0.354
1795.97	0.050	0.651	0.244	0.349
1895.77	0.048	0.655	0.254	0.345
1993.80	0.045	0.660	0.301	0.340
2178.68	0.042	0.670	0.314	0.330
2198.80	0.041	0.672	0.253	0.328
2394.22	0.038	0.677	0.230	0.323
2594.72	0.035	0.684	0.280	0.316
2794.50	0.032	0.693	0.331	0.307
2972.24	0.030	0.699	0.348	0.301
2986.31	0.030	0.702	0.330	0.298
3197.41	0.028	0.707	0.331	0.293
3237.76	0.028	0.710	0.367	0.290
3490.09	0.026	0.719	0.412	0.281
3720.84	0.024	0.730	0.428	0.270
3736.32	0.024	0.730	0.403	0.270
3996.92	0.023	0.739	0.387	0.261
4174.36	0.022	0.745	0.392	0.255
4419.45	0.020	0.751	0.425	0.249
4483.20	0.020	0.756	0.478	0.244
4734.90	0.019	0.763	0.582	0.237
4971.36	0.018	0.775	0.527	0.225
4981.98	0.018	0.777	0.500	0.223
5234.05	0.017	0.781	0.538	0.219
5471.42	0.017	0.793	0.530	0.207
5482.66	0.016	0.795	0.589	0.205
5733.71	0.016	0.801	0.496	0.199
5985.90	0.015	0.809	0.516	0.191
6236.22	0.015	0.817	0.543	0.183
6484.17	0.014	0.824	0.548	0.176
6735.21	0.013	0.831	0.549	0.169
6985.81	0.013	0.838	0.534	0.162
7471.07	0.012	0.851	0.484	0.149
7987.04	0.011	0.861	0.444	0.139
8488.61	0.011	0.870	0.485	0.130
8638.82	0.010	0.873	0.431	0.127
8771.32	0.010	0.877	0.488	0.123
8907.83	0.010	0.878	0.421	0.122
8965.36	0.010	0.880	0.424	0.120
9127.91	0.010	0.882	0.450	0.118
9294.20	0.010	0.892	0.449	0.108
9458.76	0.010	0.892	0.384	0.108
9658.47	0.009	0.893	0.441	0.107
9859.93	0.009	0.899	0.388	0.101
9966.31	0.009	0.901	0.398	0.099
10485.06	0.009	0.907	0.210	0.093
10985.13	0.008	0.908	0.277	0.092
11482.70	0.008	0.908	0.291	0.092
11982.73	0.008	0.909	0.191	0.091
12483.94	0.007	0.915	0.278	0.085
12982.38	0.007	0.915	0.288	0.085
13463.05	0.007	0.925	0.245	0.075
13982.49	0.006	0.931	0.230	0.069
14482.15	0.006	0.933	0.216	0.067
14982.25	0.006	0.935	0.231	0.065
15482.62	0.006	0.939	0.252	0.061
15980.01	0.006	0.941	0.216	0.059
16483.09	0.005	0.943	0.183	0.057
16980.39	0.005	0.945	0.180	0.055
17479.64	0.005	0.947	0.203	0.053
17978.88	0.005	0.949	0.230	0.051
18481.09	0.005	0.952	0.232	0.048
18980.01	0.005	0.953	0.251	0.047
19247.88	0.005	0.955	0.261	0.045
19477.57	0.005	0.956	0.195	0.044
19981.03	0.005	0.957	0.129	0.043
20986.79	0.004	0.959	0.121	0.041
21989.57	0.004	0.960	0.135	0.040
22990.57	0.004	0.964	0.112	0.036
22992.73	0.004	0.964	0.070	0.036
24993.90	0.004	0.965	0.097	0.035
25995.08	0.003	0.967	0.148	0.033
26995.29	0.003	0.970	0.125	0.030
27994.69	0.003	0.970	0.077	0.030
28995.14	0.003	0.971	0.070	0.029
29996.20	0.003	0.972	0.073	0.028
30995.65	0.003	0.973	0.099	0.027
31995.81	0.003	0.974	0.129	0.026
32996.19	0.003	0.976	0.093	0.024
33996.97	0.003	0.976	0.053	0.024
34997.12	0.003	0.976	0.078	0.024
35996.38	0.003	0.978	0.100	0.022
36698.42	0.002	0.979	0.069	0.021
37997.06	0.002	0.979	0.073	0.021
38997.05	0.002	0.979	0.152	0.021
39997.70	0.002	0.983	0.168	0.017
41996.21	0.002	0.985	0.089	0.015
43996.49	0.002	0.985	0.075	0.015
45639.34	0.002	0.985	0.211	0.015
45989.09	0.002	0.988	0.055	0.012
47572.09	0.002	0.991	0.063	0.009
47995.94	0.002	0.992	0.092	0.008
49995.06	0.002	0.999	0.080	0.001
51994.05	0.002	1.000	0.097	0.000
53989.27	0.002	1.000	0.014	0.000
55985.82	0.002	1.000	0.000	0.000
57985.35	0.002	1.000	0.000	0.000
59983.66	0.002	1.000	0.000	0.000
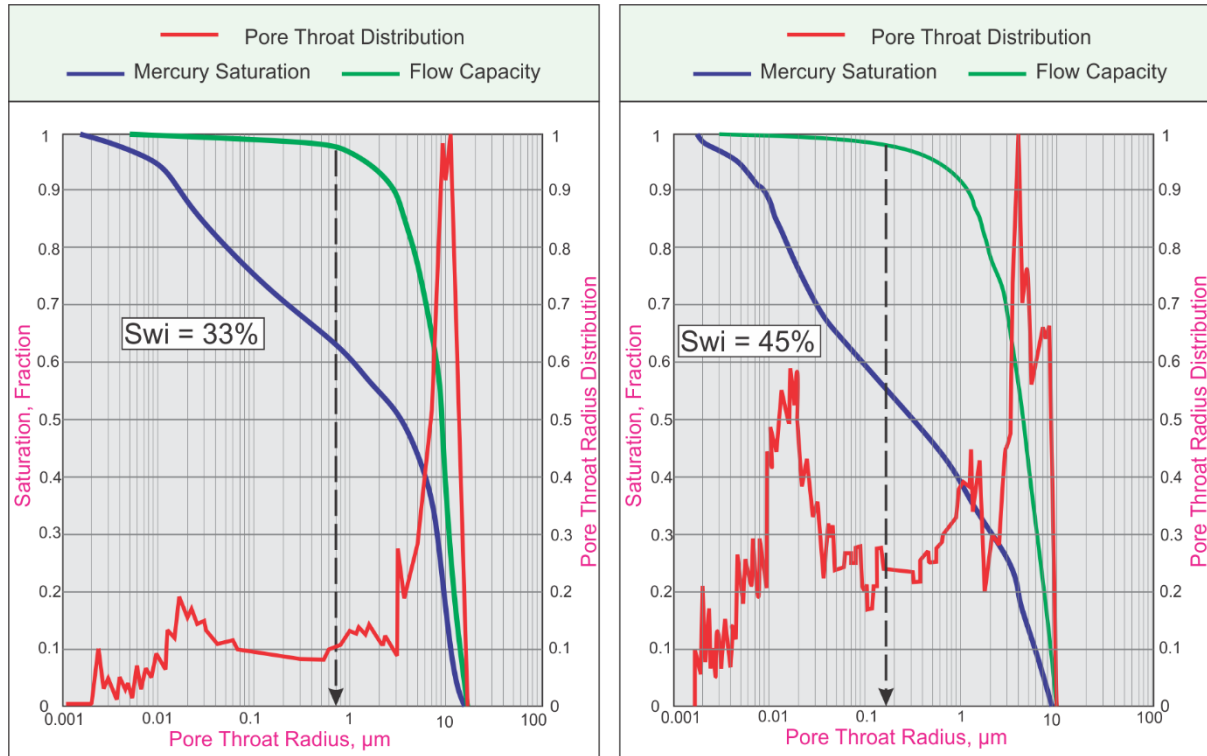
Fig. 9: Irreducible water saturation determination from MICP for Baltim North-5st well core samples.

IV. INTEGRATED PETROPHYSICAL EVALUATION.

The core data was adjusted by using of the mineralogical model, while the actual formation grain density and the determined electrical properties constants (m & n) were beneficial. The updated petrophysical evaluation allowed optimizing the production strategy on the well and propagating the same acquired information in the un-cored wells such as Baltim North-6 well.

The Baltim North -5st well (level III Main) is petrophysically considered as an unnormalized, while it can be subdivided into two intervals; the upper unit and the lower unit. The effective porosity estimated from logs for both units was lower than the lab. Core porosity was lower by an average 5.0% (the average effective porosity calculated from borehole logs was about 20% while average core porosity is about 25%). The estimated water saturation for the upper interval was equal to (Sw=50%), while it equals (Sw=65%) for the lower interval (Figure 10). After the normalization using core values and integration between the previous results of the actual core and log data, porosity difference disappeared, and excellent match was obtained.

The estimated high incorrect water saturation values from log interpretation were reduced because the calibrated log porosity was increased. Water saturation was decreased from 50 % to 30% in the upper interval and from 65 % to 50% in the lower interval.

a. Reservoir flow unit discrimination and Permeability Prediction
1.Flow Unit Definition

Flow unit is defined by Gunter, (1997) as a specific volume of reservoir, composed of one or more reservoir quality lithologies, correlative and mappable at the interval scale. A flow unit zonation is recognizable on wire-line log and may be in communication with other flow units. Flow unit is the final product of the effect of diagenetic processes on rock type. Kolodzie (1980) introduced the Winland's equation. It can be used to estimate permeability if the pore-throat radius has been independently determined. Aguilera (2002) developed the following equation for calculating pore-throat radius at 35% mercury saturation:

CPI (Logs uncalibrated)	CPI (core- calibrated logs)
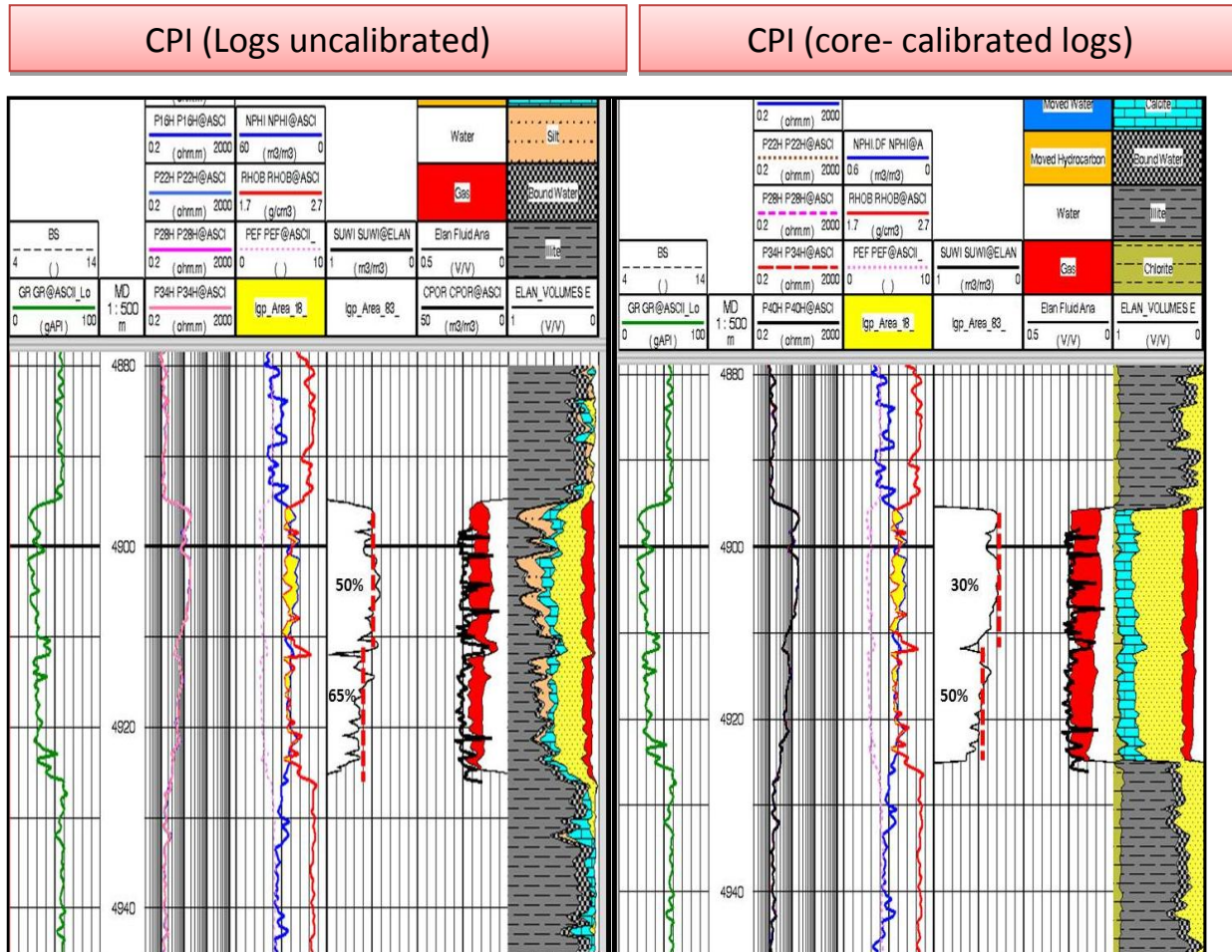
Fig. 10: Comparison between calculated water saturation using original and calibrated log by core results for the Baltim North-5st well.

$$R35 = 2.665 \ (K/Ø)^{0.45} \dots \dots \dots \dots (5)$$

Where, permeability is in mD and porosity is a percentage in both correlations.

The flow units were classified by Martine et al., (1997) into 4 flow units as;

1.   mega-port flow unit, where r35 is higher than 10 μm. (FU4)
2.   macro-port flow unit where r35 ranging between 2 and 10 μm. (FU3)
3.   mesa-port flow unit whose r35 is between 0.5 and 2 μm. (FU2)
4.   micro-port flow unit that have r35 less than 0.5 μ. (FU1)

Based on the r35 parameter, the reservoir section (level III main) penetrated by the Baltim- North-5st well has been subdivided into 3 flow units: FU4, FU3 and FU2, (Figure 11).

In particular, the above-mentioned units are characterized almost by the same range of porosity but with different permeability and grain density as illustrated in (Table 7). The better one from reservoir point of view is FU4 followed by FU3 and FU2 respectively.

2. Permeability Prediction.

Porosity- Permeability relation was constructed for each reservoir flow unit. The regression line equations (eqs.6,7&8) representing these flow units have been calculated and considered as the sole greatest approach to offer a reliable permeability in case the calculated coefficient of correlation is robust and reliable. The estimated permeability profile has been plotted along its relevant reservoirsection.
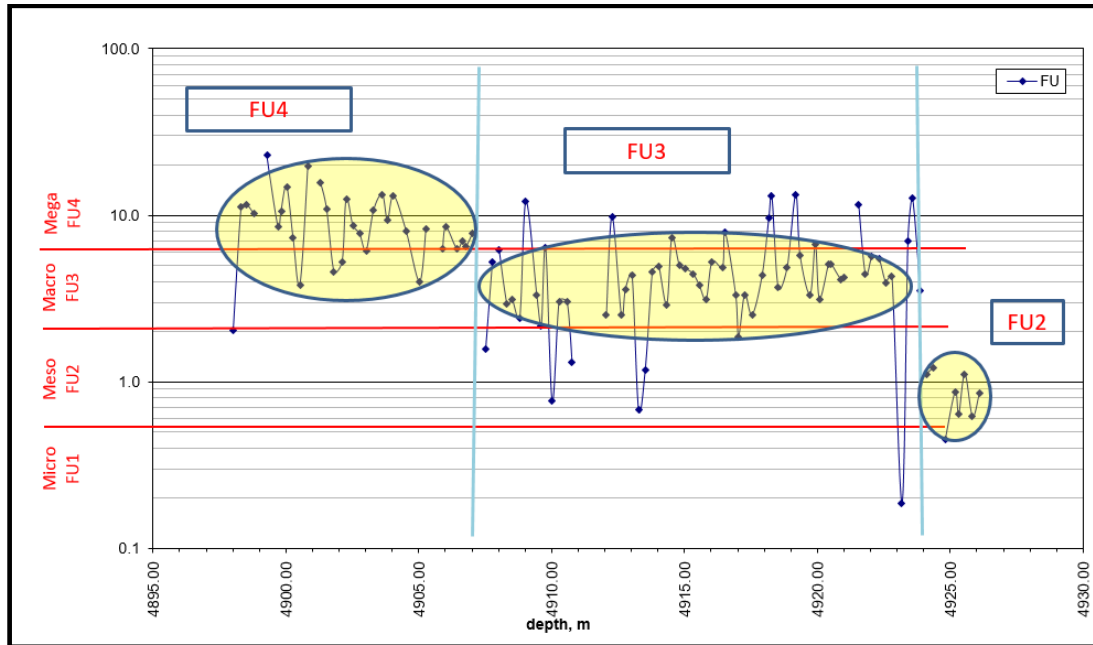
Fig. 11: Defined flow units versus depth for the Baltim North-5st cored well.

Tab. 7: Reservoir classification based on flow units and relevant petrophysical parameters in Baltim North-5st well.

FU	INTERVAL DEPTH (m)	R35 μm	POROSITY %	Horizontal Permeability md	Vertical Permeability md	Grain Density Gm/cc
FU4	4898.02-4907.77	9.1	24	308	172	2.68
FU3	4908.02-4923.86	4.8	25	123	56	2.69
FU2	4924.10-4925.83	0.9	23	5	2	2.71

This procedure is carried out only after reservoir porosity adjustment by core and log data to allowing extra robust evaluation. The resultant permeability profile (Figure 12A) for each flow unit has been resulted from core porosity and permeability altogether.

Worthy to mention that a single regression equation of permeability prediction, is not enough to expose properly of entire reservoir flow units due to their heterogeneities. (Figure 12B)

FU1 is considered as non-reservoir flow unit and therefore no regression line equation has been computed for it. In the present work, permeability was predicted (Table 8) by using the following equations for FU4, FU3, and FU2 respectively:

$$K = 1E\text{-}10 * \emptyset^{8.8377} \quad \ldots\ldots\ldots\ldots \quad (6)$$

$$K = 3E\text{-}15 * \emptyset^{11.754} \quad \ldots\ldots\ldots\ldots \quad (7)$$

$$K = 6E\text{-}14 * \emptyset^{10.19} \quad \ldots\ldots\ldots\ldots \quad (8)$$

The predicted permeability Vs core measured one (Table 8) was plotted. The resultant estimated permeability values show good agreement with core data permeability. (Track-K, Figure 15).
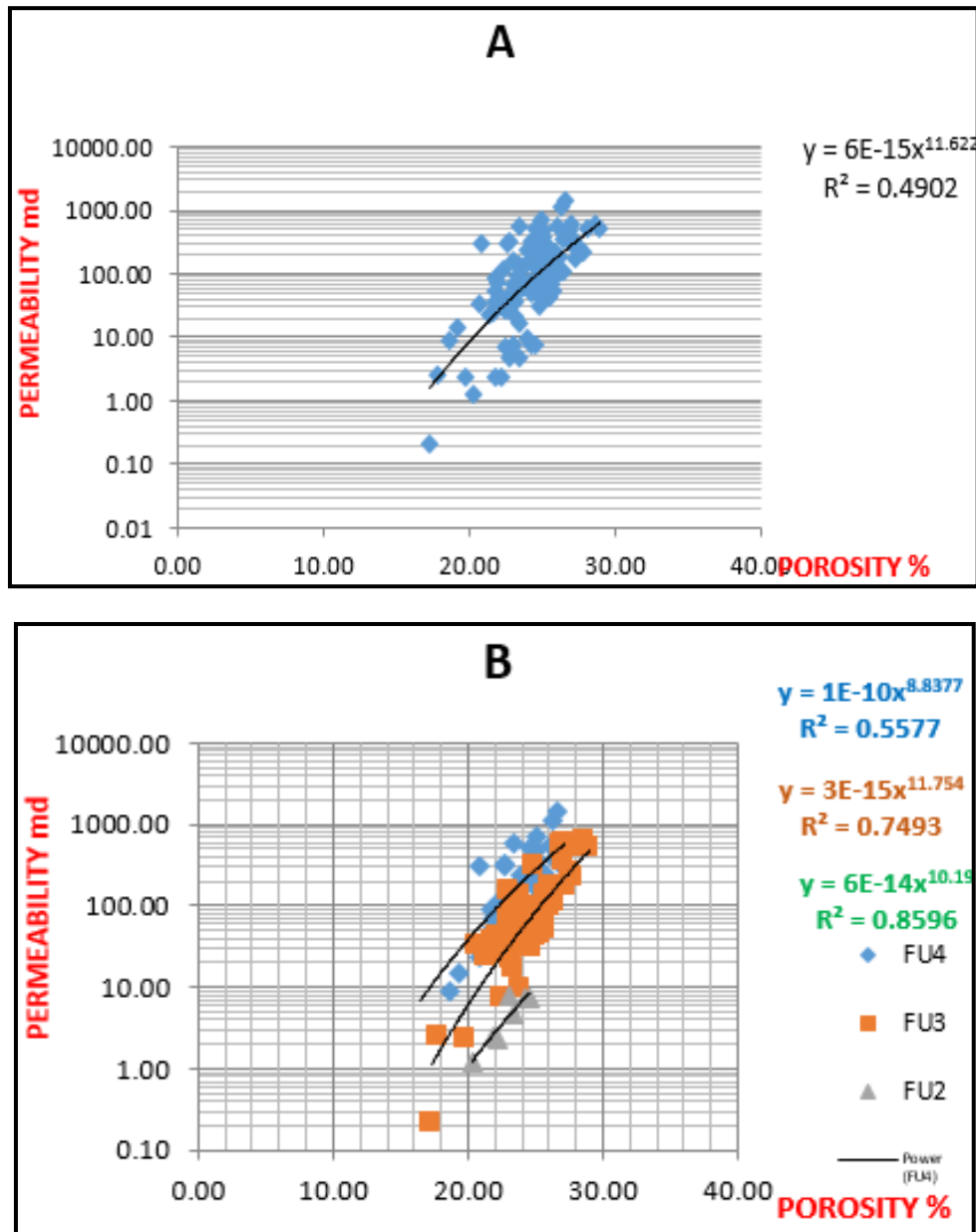
Fig. 12 A-B: Permeability prediction improvement in Baltim North-5st well.

In this graph, the mirror image between ɣ-ray log and resistivity curve indicates that the Abu Madi Formation is deposited in a deltaic fringe environment as two super imposed stream mouth bars (El Sayed, 1986).The perforated zones (Fig.13) indicates that gas production is free of associated water. It means that the water saturation is completely immovable. The clay volume is mainly chlorite and kaolinite according to XRD analysis (Fig.3).

Tab. 8: shows core porosity & core horizontal permeability and Log data Ø$_{EFF}$ and predicted permeability in Baltim North-5st well.

Sample No.	Depth	Core Data		Log Data		Sample No.	Depth	Core Data		Log Data	
		Hel. Porosity	Hor. Per	Effective Porosity	Predicted Perm.			Hel. Porosity	Hor. Per	Effective Porosity	Predicted Perm.
	m	Dec	md	Dec.	md		m	Dec	md	Dec.	md
2	4898.32	0.19	264.37	0.22	22.14	59	4912.62	0.20	33.60	0.22	220.03
3	4898.52	0.15	442.67	0.22	6.78	60	4912.77	0.20	46.66	0.22	158.71
4	4898.79	0.17	230.28	0.22	58.53	61	4913.02	0.21	68.44	0.22	56.52
5	4899.03	0.19	9.26	0.22	109.68	62	4913.27	0.22	41.21	0.22	48.66
6	4899.28	0.15	134.80	0.22	108.34	63	4913.52	0.22	9.72	0.22	49.02
7	4899.70	0.11	375.41	0.22	85.49	64	4913.79	0.22	55.50	0.22	114.85
8	4899.82	0.12	446.40	0.22	71.18	65	4914.02	0.22	99.93	0.22	175.40
9	4900.03	0.13	570.61	0.22	46.14	66	4914.33	0.24	172.27	0.22	187.05
10	4900.27	0.17	340.70	0.22	27.23	67	4914.52	0.25	217.14	0.22	191.23
11	4900.53	0.20	74.11	0.22	7.20	68	4914.80	0.26	157.15	0.22	225.93
12	4900.83	0.21	26.86	0.22	103.07	69	4915.02	0.27	102.40	0.22	254.92
13	4901.03	0.21	1.35	0.22	169.72	70	4915.32	0.26	74.75	0.22	157.89
14	4901.30	0.21	170.84	0.22	199.51	71	4915.55	0.25	58.04	0.22	79.68
15	4901.53	0.21	321.90	0.22	222.92	72	4915.81	0.24	86.93	0.22	82.43
16	4901.81	0.22	198.96	0.22	200.89	73	4916.03	0.23	111.37	0.22	84.76
17	4902.12	0.22	112.46	0.22	174.58	74	4916.43	0.25	220.81	0.22	94.37
18	4902.27	0.22	157.12	0.22	162.07	75	4916.52	0.25	245.81	0.22	96.56
19	4902.52	0.23	231.56	0.22	141.21	76	4916.92	0.26	73.23	0.22	29.38
20	4902.77	0.23	182.88	0.22	159.00	77	4917.03	0.26	21.67	0.22	9.80
21	4903.02	0.22	123.50	0.22	180.17	78	4917.26	0.25	22.82	0.22	38.21
22	4903.30	0.23	324.07	0.22	200.05	79	4917.54	0.23	30.26	0.22	76.64
23	4903.63	0.24	519.08	0.22	200.16	80	4917.92	0.24	264.99	0.22	219.13
24	4903.82	0.24	530.68	0.22	164.94	81	4918.17	0.25	266.40	0.22	262.84
25	4904.05	0.24	537.65	0.22	123.31	82	4918.28	0.25	204.87	0.22	261.75
27	4904.52	0.21	234.09	0.22	83.86	83	4918.52	0.26	70.63	0.22	259.38
29	4905.03	0.22	58.46	0.22	160.31	84	4918.86	0.25	398.72	0.22	133.43
30	4905.27	0.23	40.34	0.22	203.68	85	4919.18	0.25	436.48	0.22	47.20
31	4905.52	0.25	24.26	0.22	249.09	86	4919.34	0.24	261.54	0.22	29.49
32	4905.90	0.25	187.76	0.22	219.99	87	4919.72	0.23	43.85	0.22	90.64
33	4906.02	0.25	242.69	0.22	209.08	88	4919.92	0.24	44.94	0.22	183.18
34	4906.43	0.25	201.94	0.22	164.47	89	4920.07	0.24	49.38	0.22	226.51
35	4906.65	0.24	194.83	0.22	147.24	90	4920.42	0.25	93.45	0.22	84.14
36	4906.77	0.23	202.42	0.22	141.62	91	4920.52	0.25	106.04	0.22	43.46
37	4907.02	0.20	218.25	0.22	129.89	92	4920.87	0.24	84.44	0.22	14.92
38	4907.27	0.20	122.72	0.22	109.70	93	4921.02	0.24	73.47	0.22	5.64
39	4907.52	0.20	17.51	0.22	88.78	94	4921.32	0.25	316.70	0.22	31.56
40	4907.77	0.21	67.11	0.22	93.46	95	4921.55	0.27	501.34	0.22	53.33
41	4908.02	0.22	130.18	0.22	100.37	96	4921.80	0.26	310.72	0.22	64.30
42	4908.32	0.21	78.16	0.22	168.21	97	4922.05	0.26	126.56	0.22	73.46
43	4908.52	0.21	37.40	0.22	216.27	98	4922.31	0.25	96.05	0.22	37.91
44	4908.80	0.24	289.73	0.22	264.59	99	4922.57	0.24	64.94	0.22	9.96
45	4909.03	0.27	516.55	0.22	303.09	100	4922.80	0.22	33.26	0.22	36.75
46	4909.44	0.25	122.59	0.22	334.82	101	4923.18	0.20	151.59	0.22	144.79
47	4909.61	0.25	18.95	0.22	295.44	102	4923.40	0.22	389.47	0.22	270.65
48	4909.77	0.24	12.82	0.22	188.26	103	4923.57	0.23	508.85	0.22	330.10
49	4910.02	0.23	3.25	0.22	20.80	104	4923.86	0.25	199.48	0.22	130.60
50	4910.28	0.21	21.56	0.22	6.59	105	4924.10	0.23	6.59	0.22	6.58
51	4910.58	0.19	38.87	0.22	5.61	106	4924.36	0.21	2.81	0.22	5.73
52	4910.77	0.20	22.92	0.22	5.14	107	4924.70	0.15	1.62	0.22	3.51
53	4911.12	0.21	0.23	0.22	3.89	108	4924.81	0.18	2.59	0.22	2.38
54	4911.33	0.17	0.18	0.22	2.34	109	4925.18	0.21	5.41	0.22	0.04
55	4911.64	0.13	5.11	0.22	1.49	110	4925.31	0.20	6.14	0.22	0.04
56	4911.82	0.13	14.07	0.22	2.74	111	4925.54	0.22	7.42	0.22	0.04
57	4912.06	0.13	25.08	0.22	14.20	112	4925.83	0.20	3.18	0.22	0.04
58	4912.27	0.16	25.76	0.22	118.55	113	4926.10	0.12	0.11	0.22	0.04

3. Verification of predicted permeability models

4.1. Permeability Prediction in Baltim N-6 un-cored well.

It is important to predict permeability of the Abu Madi reservoir in un cored wells through the calculated regression line equations (6, 7 and 8) which were derived from the core data in the Baltim North-5st well.
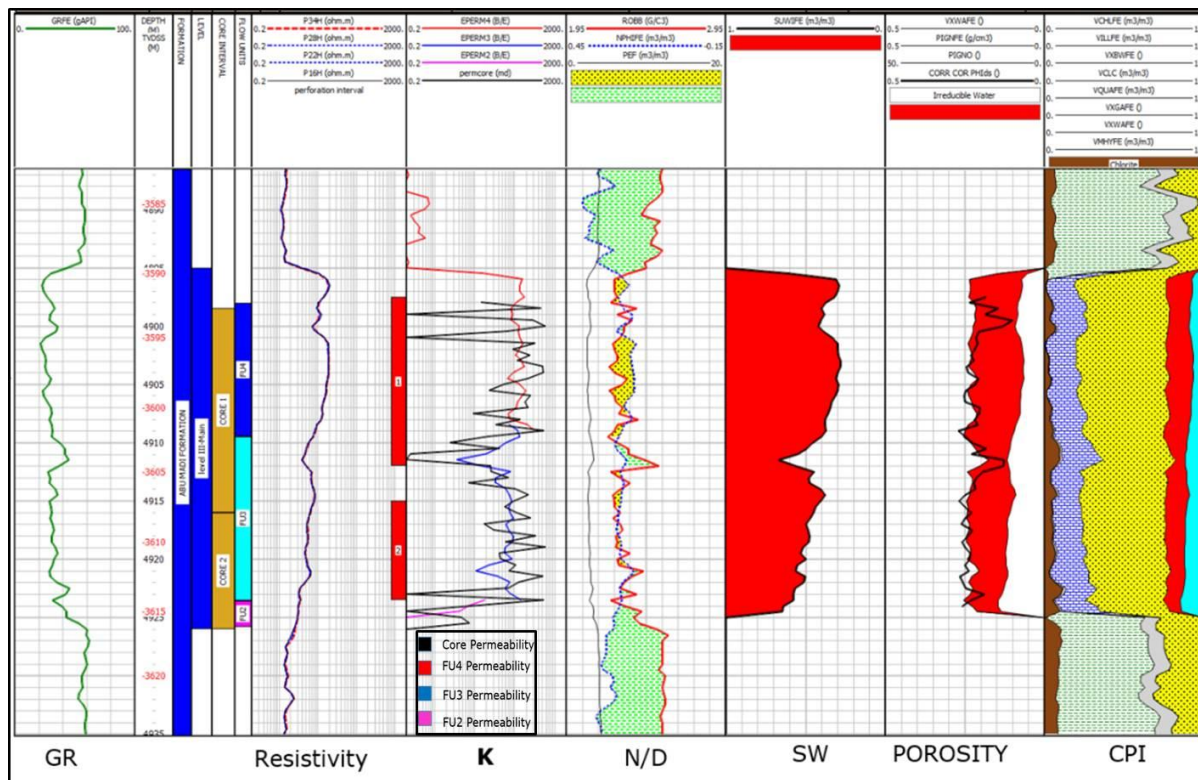
Fig. 13: From left γ-ray , depth, m, Abu Madi level III-main, core intervals -I,II-, Flow units-2,3&4 - resistivity curve (move color), perforated zones (red color),-core perm (black color), Kfu-4 (red),Kfu-3 (blue),Kfu-2 (rose)- Neutron density curves, Gas (red)/water area, gas/water area with core porosity (black), V $_{Cl}$ (brown), Carbonates (blue), Sandstone (yellow), Gas sat (red), Water Sat (bale blue).

The Abu Madi reservoir was penetrated by Baltim North-6 Well but no cores were available. Borehole logs acquired in Baltim North-6 well were GR, Resistivity and NMR. The reservoir water saturation (Sw) has been derived from the resistivity and the NMR logs, while it was high-water saturation profile in average (~ 50%). The NMR fluid discrimination, using standard T2 cutoff (33.3μs), provides a high risk of water production.

The standard T2 cutoff value for NMR in sandstone reservoirs must be normalized depending on sandstone pore size distribution and geometry, which is exactly the case shown in this study.(Akkurt, et al., 2008, El-Sayed&Nahla, 2016, Chen, et al., 2017 and Cheng et al. 2017).The T2 cutoff value in the Baltim North-6 well has been modified from 33.3 μs to 150 μs. This was done through numerous iterations starting with T2 = 50,100 up to 150 μs and the last was the most reliable to calculate permeability and water saturation from NMR log. According to the pore throat size distribution (PTSD) calculated from the MICP investigation of the Baltim North-5st well core (Tables 5,6&7) side by side with NMR lab analysis, the synchronization allowed obtaining better permeability and water saturation estimation in Baltim North-6 well. (Table 9) and (Figures 14 & 15).

The resistivity (saturation exponent) and gamma ray logs have been used as bridge for application of the flow unit concept for the Baltim North-6 well. Starting from that previously defined on Baltim North-5st well core data and related to its log dataset, FU4 and FU3 were detected in the reservoir section of new Baltim North-6 well.

Tab. 9: NMR and flow unit predicted permeability in Baltim North-6 well.

DEPTH	NMR_K_33.3	NMR_K_150	K_Prediced	SUWI_NMR	SW
m	md	md	md	Dec	Dec
4100.04	0.04	0.01	0.04	1.00	0.89
4100.54	0.26	0.32	0.15	1.00	0.76
4101.04	0.38	0.71	1.14	1.00	0.78
4101.54	0.44	0.85	0.68	0.78	0.76
4102.04	0.22	0.49	1.69	0.56	0.81
4102.54	0.19	0.57	2.60	0.55	0.81
4103.04	0.54	5.49	4.82	0.69	0.67
4103.54	0.55	3.27	2.39	0.98	0.69
4104.04	0.54	1.18	1.81	0.53	0.76
4104.54	1.70	11.70	7.28	0.55	0.64
4105.04	3.11	30.18	35.86	0.53	0.53
4105.54	4.15	48.80	41.16	0.52	0.48
4106.04	4.45	39.84	21.00	0.52	0.51
4106.54	3.16	30.80	23.63	0.50	0.52
4107.04	1.82	8.97	9.55	0.48	0.59
4107.54	3.17	15.14	42.16	0.50	0.59
4108.04	1.34	6.54	15.47	0.49	0.68
4108.54	1.48	4.94	15.05	0.50	0.71
4109.04	2.08	13.29	55.66	0.52	0.62
4109.54	1.68	25.51	61.70	0.52	0.56
4110.04	1.98	35.50	50.14	0.52	0.54
4110.54	2.44	31.98	34.88	0.50	0.49
4111.04	3.02	32.89	39.54	0.52	0.48
4111.54	3.26	36.45	62.88	0.53	0.49
4112.04	3.12	53.06	73.31	0.53	0.52
4112.54	2.64	42.91	48.98	0.53	0.50
4113.04	2.10	58.91	89.66	0.55	0.51
4113.54	1.00	28.74	19.30	0.53	0.56
4114.04	1.04	8.03	22.12	0.54	0.67
4114.54	1.41	25.47	27.78	0.54	0.60
4115.04	1.55	16.89	34.93	0.54	0.59
4115.54	1.40	9.16	23.20	0.52	0.62
4116.04	1.13	6.13	6.02	0.50	0.65
4116.54	1.17	9.77	8.01	0.53	0.63
4117.04	1.67	14.14	11.15	0.51	0.59
4117.54	1.42	8.60	4.44	0.49	0.59
4118.04	2.07	13.53	11.44	0.52	0.57
4118.54	2.90	40.62	14.52	0.54	0.49
4119.04	1.67	35.65	15.79	0.51	0.53
4119.54	0.79	14.21	13.87	0.51	0.62
4120.04	0.92	8.19	17.94	0.52	0.66
4120.54	0.33	1.91	0.59	0.57	0.73
4121.04	0.21	0.52	0.26	0.47	0.78
4121.54	1.72	13.62	38.29	0.52	0.57
4122.04	2.84	70.03	82.48	0.54	0.51
4122.54	1.99	23.37	50.53	0.56	0.59
4123.04	2.22	60.94	70.90	0.56	0.53
4123.54	1.27	14.03	5.71	0.47	0.50
4124.04	1.57	29.45	4.89	0.51	0.52
4124.54	1.59	16.48	30.82	0.55	0.64
4125.04	0.79	6.56	8.88	0.54	0.66
4125.54	0.28	0.85	2.43	0.53	0.81
4126.04	2.10	10.81	26.72	0.56	0.65
4126.54	0.22	1.33	2.46	0.52	0.82
4127.04	0.31	1.34	2.53	0.54	0.82
4127.54	0.32	1.34	2.77	0.57	0.82
4128.04	0.71	6.61	16.05	0.83	0.78
4128.54	1.11	26.34	50.84	1.00	0.74
4129.04	0.83	8.68	13.29	1.00	0.73
4129.54	0.05	0.17	-999.00	1.00	0.87
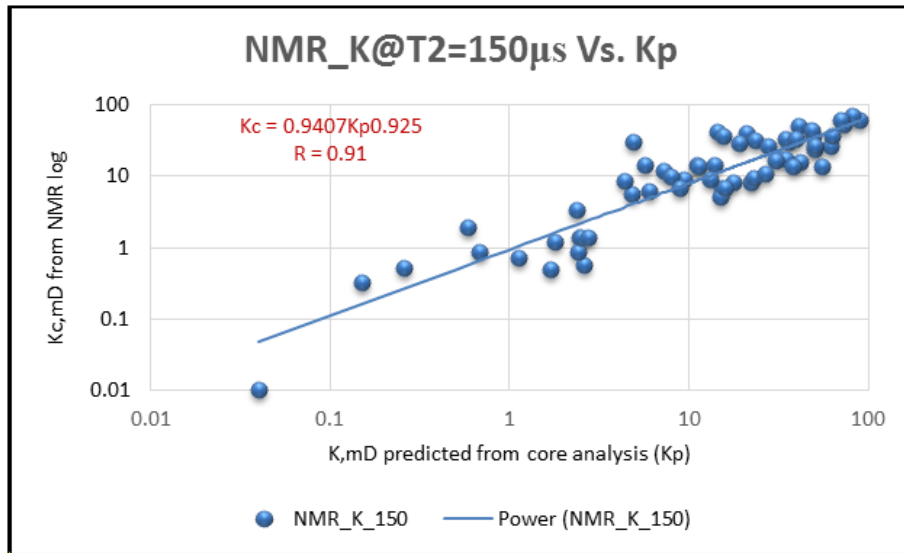
Fig. 14:Predicted permeability from core analysis versus permeability at NMR T2-cutoff (150 µs), Baltim North-6 well.
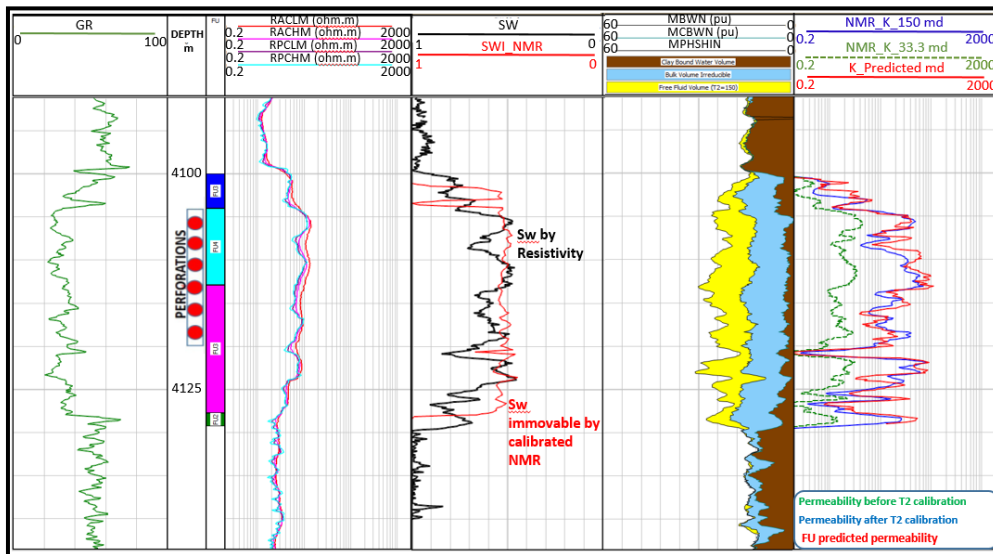
Fig. 15: The predicted permeability from core analysis data (red color curve and NMR @ 150 and 33.3 µm permeability (blue &green color curves); Clay bound water (CBW-_dark brown area), BVI (micro porosity-blue area), BVM (Mobile fluids- yellow area), Swi calculated from resistivity curve (black) and normalized NMR (red color curve) for the Baltim North-6 well.

The red curve (Figure 15) is the predicted permeability based on core analysis data of flow units in Baltim North-5 and the blue curve is the predicted permeability from NMR log T2-cutoff= 150 µs. The green curve is the predicted permeability from NMR log at T2-cutoff= 33.3 µs.

A comparison has been made between the NMR derived permeability at the standard T2 cutoff (33.3 µs) and permeability at the calibrated T2-cutoff (150 µs). It shows a very close   (R = 0.94) agreement but a very large difference in permeability values.

This discrepancy among permeability results was the reason that the standard NMR-relaxation time for sandstone (T2 = 33.3 µs) was not convenient or suitable for the Abu Madi sandstone reservoir. It gave unreliable permeability profile in non-cored wells. (Figure 16)
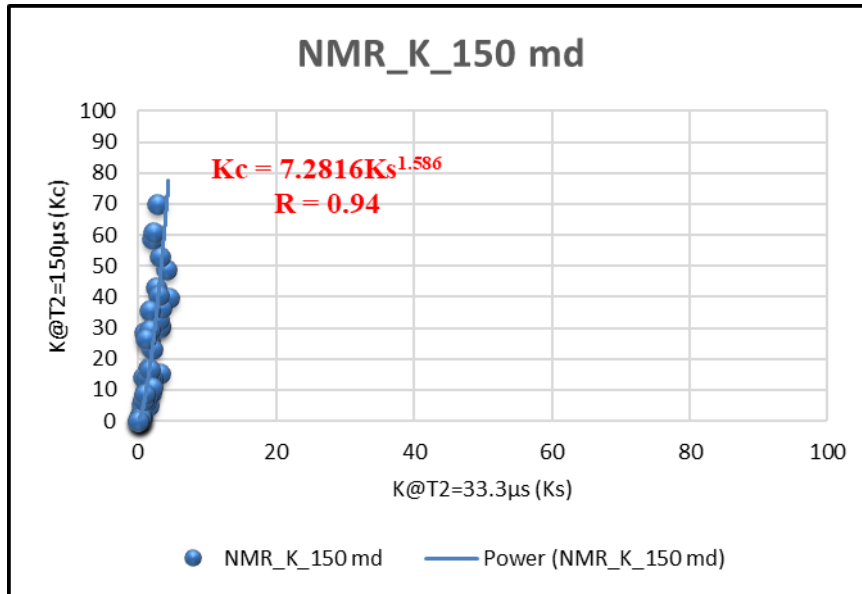
Fig. 16: comparison between the NMR derived permeability at the standard T2 cutoff (33.3 μs) and permeability at the calibrated T2-cutoff (150 μs), Baltim North-6 well.

According to the Abu Madi reservoir production data (Table 10), the obtained highly water saturation values that could affects the reservoir production was most likely due to the immobile water (CBW + BVI). The production data has shown very low water cut in the produced gas, which means that the estimated water saturation from the open hole logs was not accurate and has to be re-evaluated. Therefore, no risks of early water cut are expected in putting this zone in production.

The production data, used as blind test, showed very good agreement with petrophysical analysis.

Tab. 10: Production data for Baltim North-6 well.

Date	Calendar Day Gas Vol. Prod MMcf/d	Cus Gas Vol. Prod B	Date	Calendar Day Gas Vol. Prod MMcf/d	Cus Gas Vol. Prod B
30-Jun-17	4.54	107.64	**31-Jul-18**	2.33	108.89
31-Jul-17	4.42	107.77	**31-Aug-18**	1.82	108.94
31-Aug-17	4.11	107 90	**30-Sep-18**	2.65	109.02
30-Sep-17	3.96	108 02	**31-Oct-18**	3.58	109.13
31-Oct-17	3.58	108.13	**30-Nov-18**	4.39	109.27
30-Nov-17	2.44	108.20	**31-Dec-18**	3.89	109.39
31-Dec-17	2.75	108.29	**31-Jan-19**	3.86	109.51
31-Jan-18	3.36	108.39	**28-Feb-19**	3.67	109.61
28-Feb-18	3.21	108.48	**31-Mar-19**	3.76	109.72
31-Mar-18	2.95	108.57	**30-Apr-19**	3.89	109.84
30-Apr-18	2.78	108.66	**31-May-19**	3.80	109.96
31-May-18	2.65	108.74	**30-Jun-19**	2.83	110.04
30-Jun-18	2.47	108.81	**31-Jul-19**	2.85	110.13
			31-Aug-19	2.76	110.22

The gas production in Baltim North-6 well started from Level III Main in year 2015 with rate 9 MMcf/d (without water cut). The gas production decreased gradually and still producing with 3 MMcf/d, validating the formation evaluation workflow adopted in this work, (Figure 17).
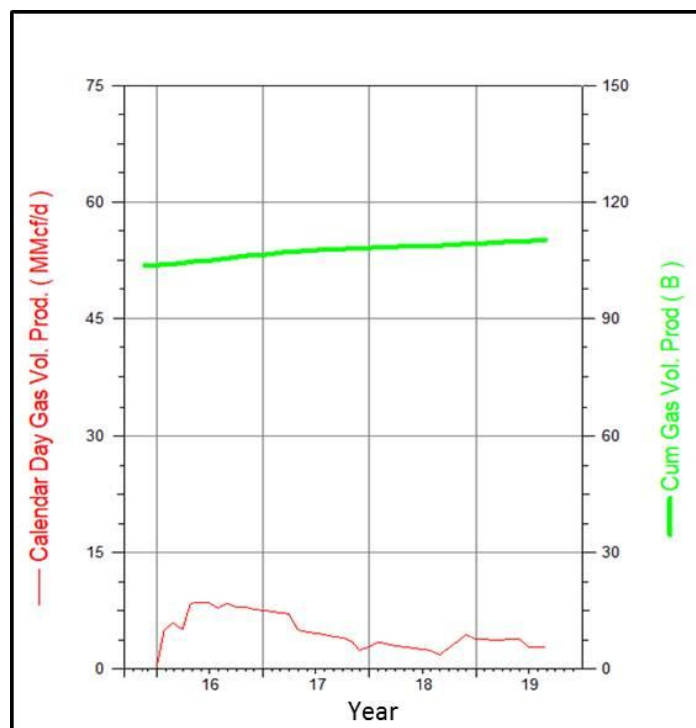
Figure 17: Production Performance for well Baltim North-6.

V. CONCLUSION

1. The environment of deposition of Abu Madi Formation is mainly deltaic fringe deposits and represented by two superimposed stream mouth bars.
2. The majority of Abu Madi samples are mainly composed from quartz, some feldspar and oxidizing glauconite as detrital grains and cemented by calcite and Ferron calcite. The predominant clay minerals were chlorite and kaolinite.
3. The Abu Madi calculated cementation factor (m) and saturation exponent (n) are equal 1.45 & 1.81 at ambient and 1.61 & 1.96 at overburden reservoir pressure respectively.
4. The measurements of pore throat size distribution, saturation exponent and production history are essential to normalize NMR-T2 cut-off for sandstone reservoirs in borehole logs and determination of micro-porosity and irreducible water saturation.
5. The flow unit approach in cored wells is necessary for NMR normalization and predicting permeability profile in un-cored wells in the same field.
6. Integration core analysis derived parameters and detection of flow units have strongly enhancing the reservoir synergy and petrophysical evaluation.

REFERENCES

[1]. Aagaard, P., Jahren, J., 2010. Special issue introduction: compaction processes –porosity, permeability and rock properties evolution in sedimentary basins.Mar. Petrol. Geol. 27, 1681–1683.
[2]. Al Khalifa,H., P.W.J. Glover, P. Lorinczi, 2020: Permeability prediction and diagenesis in tight carbonates using machine learning techniques. Marine and Petroleum Geology 112 (2020) 104096.
[3]. Akkurt, R., Seifert, D., Al-Harbi, A., Al-Beaiji, T. M., Kruspe, T., Thern, H., and Kroken, A. 2008: Real-Time Detection of Tar in Carbonates Using LWD Triple Combo, NMR and Formation Tester in Highly-Deviated Wells. Proceeding of 49th Annual Logging Symposium, Austin, Texas, 25-28.
[4]. Chen, J.-H., Althaus, S. M., Delshad, M., Zhang, J., Almalki, F., Sun, Q., and Shawaf, A., 2017: Optimization of NMR Permeability Transform and Application to Middle East Tight Sands. SPAWLA-58th.
[5]. Cheng, Y., Chen, S., Eid, M., Hursan, G., and Ma, S., 2017: Determination of Permeability From NMR T1/T2 Ratio in Carbonates. SPAWLA -58th.
[6]. El Diasty, W.Sh., 2010. Organic Geochemistry and Hydrocarbon Potentiality of the Subsurface Miocene – Pliocene Succession in the Northwestern Part of the Nile Delta. Unpublished Ph. D Thesis, Geology Department, Faculty of Science, Mansoura University, 303 pp.
[7]. El Diasty, W.Sh. a, K.E. Peters , J.M. Moldowan , G.I. Essa , M.M. Hammad ,(2020): Organic Geochemistry of condensates and natural gases in the northwest Nile Delta offshore Egypt, Journal of Petroleum Science and Engineering 187 (2020) 106819
[8]. El Heiny I., Rizk, R., and Hassan, M., 1990: Sedimentological mode for Abu Madi Reservoir sands, Abu Madi Field, Nile Delta, Egypt. EGPC, 10th Petrol. Expl. Prod. Conf., Cairo, vol. 2, p. 515 – 551.
[9]. EL-SAYED, A.M.A (1986): Delineation of charged deltaic rock genetic types in Algyo-2 hydrocarbon reservoir ,Hungary based on log curve shapes. Sci. Bull. (1986), 6 : 257- 271

[10]. El Sayed, Abdel Moktader A., 1993: Intercorrelation of capillary pressure derived parameters for sandstones of the Tortel Formation, Hungary. Journal of Petroleum Science and Engineering, 10 (1993) 47-53.

[11]. El Sayed, A.M. A. ,Makary,S. and Salah,A.(2005): Microporosity:A New definition based on pore throat size.,InternationalConf.onThethys Geology, 12-14 Nov. Cairo Univ.V.I. P. 257.

[12]. El Sayed, A. A. and N. A. El Sayed, 2016: Petrophysical Properties of Clastic Reservoirs Using NMR Relaxometry and Mercury Injection Data Bahariya Formation. Egypt IOP Conf. Ser.: Earth Environ. Sci. 44 042018.

[13]. Glover, P.W.J., Zadjali, I., Frew, K., 2006. Permeability prediction from MICP and NMR data using an electro-kinetic approach. Geophysics 71, F49–F60.

[14]. G.W. Gunter, J.M. Finneran, D.J. Hartman, J.D. Miller, Early determination of reservoir flow units using an integrated petrophysical method, SPE 38679, in: SSPE Annual Technical Conference and Exhibition. San Antonio, TX; October 5–8, 1997, 1997.

[15]. Halisch, M., A.Weller, Carl-Sattler, W. Debschütz and Abdel Moktader El-Sayed,(2009): A Complex Core-Log Case Study of an Anisotropic Sandstone, Originating from Bahariya Formation, Abu Gharadig Basin, Egypt. PETROPHYSICS, VOL. 50 NO. 6 (DECEMBER 2009); Page 478-497; 21 Figures; 7 Tables

[16]. Haoran Xia, Elizabeth Hernandez Perez, Thomas L. Dunn: The impact of grain-coating chlorite on the effective porosity of sandstones, Marine and Petroleum Geology 115 (2020) 104237

[17]. Kolodzie, S., Jr., 1980, Analysis of pore-throat size and use of the Waxman-Smits equation to determine OOIP in Spindle Field, Colorado: Society of Petroleum Engineers, SPE-9382-MS, 10p.

[18]. Lala , Amir Maher Sayed; Nahla A.A. El-Sayed (2017): Controls of pore throat radius distribution on permeability Journal of Petroleum Science and Engineering 157 (2017) 941–950.

[19]. Martin, A.J., S.T. Solomon, and, D.J. Hartmann, 1997: Characterization of petrophysical flow units in carbonate reservoirs. AAPG Bulletin, v.81, no.5, May 1997, p. 734-759.

[20]. R. Aguilera, Incorporating capillary pressure, pore aperture radii, height above free water table, and Winland r35 values on Pickett plots, Am. Assoc. Petrol. Geol. Bull. 86 (4) (2002) 605.

[21]. RikkeWeibel, MetteOlivariusa,, Lars Kristensena, HenrikFriis, Morten LethHjulera,ClausKjøller, Anders Mathiesen, Lars Henrik Nielsen (2017) Predicting permeability of low-enthalpy geothermal reservoirs: A case study from the Upper Triassic – Lower Jurassic Gassum Formation, Norwegian–Danish Basin, Geothermics 65 (2017) 135–157.

[22]. Rizzini A., Vezzani, F., Cococcetta, V., and Milad, G., 1978: Stratigraphy and Sedimentation of a Neogene-Quaternary section in the Nile Delta area, (A.R.E.). Mar. Geol., vol. 27, p.327 - 348.

[23]. Wei Meng , ZichengNiu, Yang Hu, Tianxia An , Keqi Liu , Gao Qiang,2020: Genesis of authigenic kaolinite and its indicative significance to secondary pores in petroliferous basins: A case study in the Dongying Sag, Bohai Bay Basin, Eastern China,: Journal of Petroleum Science and Engineering.

[24]. Xuqiang, Fana, GuiwenWanga, Yafeng, Lic, Quanqi, Daia,SongLinghud, ChaoweiDuand,ChengenZhangd, FengshengZhangd, 2019: Pore structure evaluation of tight reservoirs in the mixed silici- clastic carbonate sediments using fractal analysis of NMR experiments and logs. Marine and Petroleum Geology 109 (2019) 484–493.

[25]. Zhu, L., Zhang, C., Wei, Y., Zhang, C., 2017a. Permeability prediction of the tight sandstone reservoirs using hybrid intelligent algorithm and nuclear magnetic resonance logging data. Arab. J. Sci. Eng. 42, 1643–1654. https://doi.org/10.1007/s13369-016-2365-2.